Research Article

Journal of Environmental Nanotechnology

Sensing 6-Mercaptopurine with a Thiophene-carbazole Copolymer Matrix: A First Principles Approach

Pooja Sharma[1,3*], Reena Srivastava[2], Anurag Srivastava[3] and Rachana Kathal[1]

[1]Department of Applied Chemistry, Amity University, Maharajpura Dang, Gwalior, MP, India

[2]SOS in Chemistry, Jiwaji University, Gwalior, MP, India

[3]Material synthesis and Sensor Design (MSSD) Lab, Department of Engineering Sciences, ABV Indian Institute of Information Technology and Management, Gwalior, MP, India

Received: 24.04.2024 Accepted: 23.05.2024 Published: 30.06.2024

*poojasharma1243@gmail.com

ABSTRACT

This study discusses the impact of cytostatic drugs, particularly 6-mercaptopurine(6-MP), as emerging pollutants in aquatic ecosystems. Computational analyses using Density Functional Theory analyzed the electronic properties and adsorption behavior of the 3-methoxy thiophene (3-MeOTH) monomer matrix and the 3-methoxy thiophene(3-MeOTH)–n-vinyl carbazole (NVK) copolymer matrix in the presence of 6-MP. Results indicate that 6-MP is adsorbed on the matrices of 3-MeOTH polymer and 3-MeOTH-NVK copolymer with weak Van der Waal forces as indicated by negative adsorption energy and a significant charge transfer. Additionally, 6-MP shows notable sensitivities with both matrices, with 3-MeOTH-NVK demonstrating a 37.8% higher sensitivity compared to 3-MeOTH polymer. Enhanced conductance and peak amplitude enhancements in the presence of 6-MP suggest the potential of these materials for drug sensing applications.

Keywords: Density functional theory; 6-mercaptopurine; 3-methoxy thiophene; N-vinyl carbazole; Emerging pollutants.

1. INTRODUCTION

Recently identified synthetic or natural substances that enter the biological systems of humans and animals with limited regulatory oversight, called emerging pollutants (EPs) pose a challenge in environmental management (Saboorizadeh *et al.* 2021). Despite their presence from trace levels to high concentrations in aquatic systems, they show significant adverse impact on the ecosystems because EPs lack comprehensive monitoring protocols or legislative frameworks (Mousavi *et al.* 2020). Among these emerging contaminants, cytostatic drugs used in chemotherapy have become particularly concerning environmental pollutants due to their genotoxic properties and resistance to degradation (Santana *et al.* 2016). Notably, 6-mercaptopurine (6-MP), a widely utilized cytostatic agent to treat acute lymphocytic leukemia, poses a specific hazard due to its low biodegradability requiring advanced oxidation processes for its effective removal (Ensafi *et al.* 2012; González *et al.* 2021). The limited research available underscores the critical need for further investigation into the occurrence, environmental fate and ecological effects of cytostatic drugs. Developing comprehensive studies to assess their presence, concentration and impact on the environment after disposal is crucial in understanding and mitigating the risks they pose to aquatic ecosystems and human health.

The precise identification of anticancer drugs in aquatic environments holds significant importance, driving extensive research efforts towards developing efficient detection materials. Carbon quantum dots are a promising material for detecting 6-MP drug residues. Numerous studies have explored the efficacy of carbon quantum dots across varied sample matrices. Amine-functionalized and fluorescent carbon quantum dots, multiwall carbon nanotubes-TiO_2 hybrids(González *et al.* 2021), ZnO–graphene capped quantum dots embedded in polymer matrices have been employed as fluorometric sensors for aqueous and biological samples (Agrawal *et al.* 2021; 2022; Ensafi *et al.* 2012; Ipte *et al.* 2023; Mousavi *et al.* 2020) Additionally, investigations have extended to alternative materials like conjugated structures, namely, Fe_3O_4@polypyrrole-Pt core-shell nanoparticles for the detection of 6-MP (Hatamluyi et al. 2018). These diverse approaches reflect ongoing efforts to synthesize robust and adaptable detection materials for 6-MP in various environmental and biological contexts, addressing crucial requirements in environmental surveillance and medical applications. Nevertheless, there exists a research gap concerning the utilization of conjugated materials like aniline, carbazole, acetylene, and thiophene for 6-MP detection. Thiophene and n-vinyl carbazole, notable among these materials, due to their synthetic flexibility and favorable optoelectronic properties, offer distinct advantages. Thiophene and its derivatives facilitate polymer backbone planarization, carbazole and its nitrogen-containing aromatic

heterocyclic derivatives find broad applications across industries, including pharmaceuticals and light-emitting photosensors (Sharma *et al*. 2023; Tajik *et al*. 2021). Consequently, this research embarks on a comprehensive comparative analysis of the sensing ability of 3-MeOTH and its copolymer with n-vinyl carbazole (3-MeOTH-NVK), through studying their electronic properties and adsorption behavior using Density Functional Theory (DFT).

2. COMPUTATIONAL DETAILS

The Density Functional Theory was performed to analyze the structural and electronic properties of synthesized polymer matrices. The analysis exploited the Perdew-Burke-Ernzerhof (PBE) functional within the generalized gradient approximation (GGA), applying double-zeta-polarized (DZP) basis sets for optimization. Matrices were optimized until forces on each atom reached below 0.05 eV/Å. A Rydberg cut-off energy of 75 and convergence threshold energy of 10^{-5} eV were chosen, alongside a K-point sampling of 1×1×1 for accurate calculations of Molecular Energy Spectrum (MES) and Density of States (DOS).

A device simulator with gold (Au) electrodes was used to calculate the transmission spectrum of synthesized polymer matrices. The PBE function with local density approximation (LDA), 75 Hartee cut-off energy and 3×3 K-point are applied for optimization of the device.

3. RESULTS AND DISCUSSION

In this study, we analyzed the most stable optimized geometries among various orientations to conduct a comprehensive analysis of the electronic properties of 6-mercaptopurine adsorbed onto both 3-MeOTH and its copolymer 3-MeOTH-NVK.

3.1 Stability Analysis

To understand the interaction between the 3-MeOTH-NVK and 3-MeOTH with the 6-MP drug, the adsorption energy of both 3-MeOTH+6-MP and 3-MeOTH-NVK+6-MP systems was computed and analyzed using equation 1 (Table 1) (Agrawal et al. 2022). The calculated adsorption energy values for 3-MeOTH and 3-MeOTH-NVK with 6-MP drug are -1.918 eV and -3.173 eV, respectively. The negative value of the adsorption energy indicates an exothermic reaction and weak Van der Waals interaction between both the systems. This interaction is illustrated in Fig.1, where after full relaxation, the distance of 6-MP from 3-MeOTH and 3-MeOTH-NVK systems was found to be 3.33 Å and 2.85 Å, respectively. This distance, defined as the molecule-drug distance, represents the minimum atom-to-atom distance between the molecule and the drug.

The comparison between both the systems reveals that 3-MeOTH-NVK exhibits a significantly higher release of interaction energy, precisely 65.43% more than that of 3-MeOTH. This suggests that the 3-MeOTH-NVK copolymer is more stable than the 3-MeOTH monomer. Furthermore, due to the weak Van der Waals interaction between the drug and the molecule, no significant changes are observed in their geometry. Consequently, the bond length of the molecules remains nearly unchanged after the adsorption of 6-MP.

$$E_{ads} = TE_{(matrix+6\text{-}MP)} - (TE_{(matrix)} + TE_{(6\text{-}MP)}) \quad \ldots\ldots (1)$$

Here, E_{ads}, $TE_{(matrix+6\text{-}MP)}$, $TE_{(matrix)}$ and $TE_{(6\text{-}MP)}$ are adsorption energy, energy of optimized molecule-6-MP system and energy of 6-MP drug, respectively.

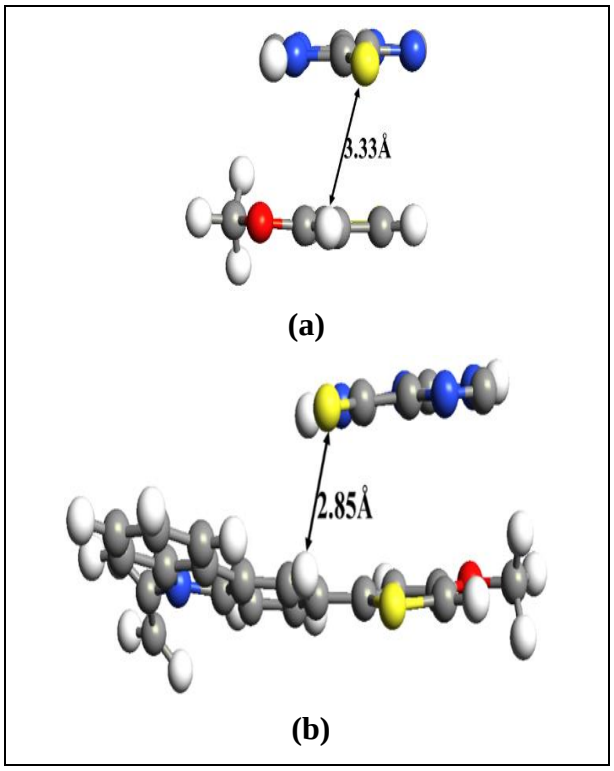

Fig. 1: Schematic view of 6-MP drug adsorption on studied matrices (a) 3-MeOTH monomer, (b) 3-MeOTH-NVK copolymer

3.2 Electron Density Analysis

The charge transfer between the drug and the molecule was computed through Mulliken population analysis using equation 2 (Table 1) (Agrawal *et al.* 2022). Notably, the 3-MeOTH-NVK+6-MP system shows almost double the charge transfer to 6-MP compared to the 3-MeOTH+6-MP system. Specifically, 0.053e is transferred from 3-MeOTH to 6-MP, while 0.106e is transferred from 3-MeOTH-NVK to 6-MP. Fig. 2 presents the electron density and positioning of 6-MP on 3-MeOTH and 3-MeOTH-NVK, where the jade-green color indicates the significant accumulation of electron

densities on nitrogen and oxygen atoms due to their electronegative nature.

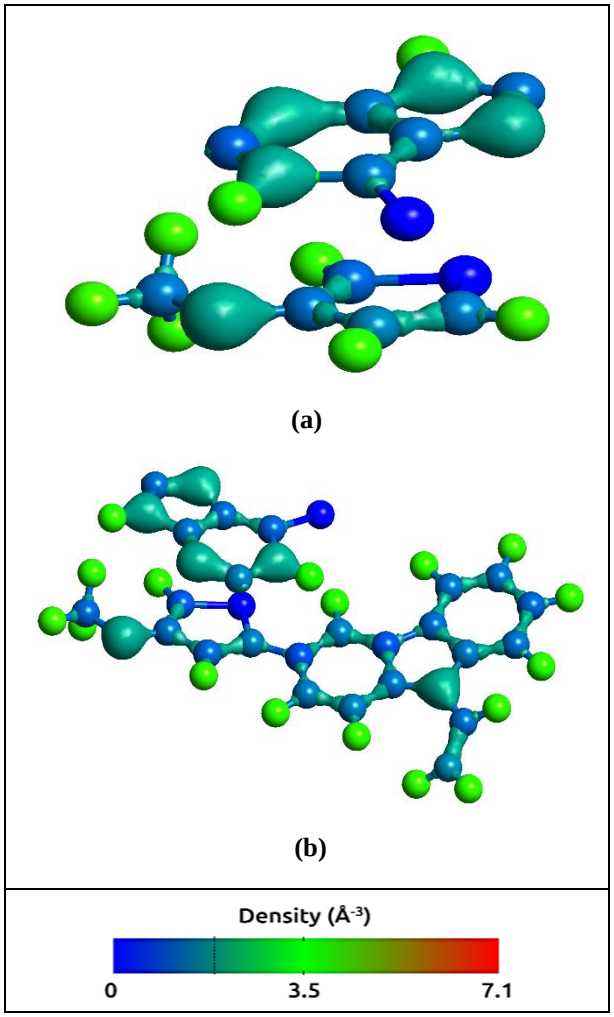

Fig. 2: Schematic view of electron densities of 3-MeOTH+6-MP (a) and 3-MeOTH-NVK+6-MP (b) systems at isoscales value of 1.9

$$\Delta\rho = \rho_{(\text{matrix}+6-\text{MP})} - \rho_{(6-\text{MP})} \quad \text{..... (2)}$$

Here $\Delta\rho$, $\rho_{(\text{matrix+6-MP})}$, and $\rho_{(6\text{-MP})}$ are charge transfer, charge on 6-MP after adsorption on the matrix, and charge on 6-MP before adsorption on the matrix, respectively.

Table 1. Calculated adsorption energies and Mulliken charges of the 3-MeOTH+6MP and 3-MeOTH-NVK+6MP systems

System	E_{ads}	Q(e)[1]
6-MP on 3-MeOTH-NVK	-3.173	0.106e
6-MP on 3-MeOTH	-1.918	0.053e

3.3 Electronic Properties Analysis

The molecular orbital analysis highlights the significant influence of 6-MP adsorption on the HOMO-LUMO (E_H-E_L) gap for both 3-MeOTH and 3-MeOTH-NVK molecules. Upon 6-MP adsorption, the E_H-E_L gap of 3-MeOTH decreases from 4.08 eV to 0.2 eV, while 3-MeOTH-NVK experiences a reduction from 2.8 eV to 0.1 eV. A comparison reveals that the 3-MeOTH-NVK+6-MP system has half the E_H-E_L gap of the 3-MeOTH+6-MP system, confirming the respective reduction of the E_H-E_L gap. This reduction is evident in the shifting of HOMO and LUMO energy levels towards the Fermi level (Fig. 3). A smaller E_H-E_L gap indicates a good conductive behaviour of systems. Additionally, the impact of 6-MP on the 3-MeOTH and 3-MeOTH-NVK matrices was analyzed by computing its DOS profile. The right panel of Fig. 3 provides insight into the DOS profiles for 3-MeOTH and 3-MeOTH-NVK before and after the adsorption of 6-MP. The DOS profile for both molecules support the observed changes in the E_H-E_L gap, with successive shifts of DOS curve near the Fermi level. Remarkably, the DOS plot of both molecules after the interaction with 6-MP shows remarkable changes in the position, count, and strength (height) of peaks due to alteration in the electronic property, further emphasizing the robustness of the studied systems for drug sensing.

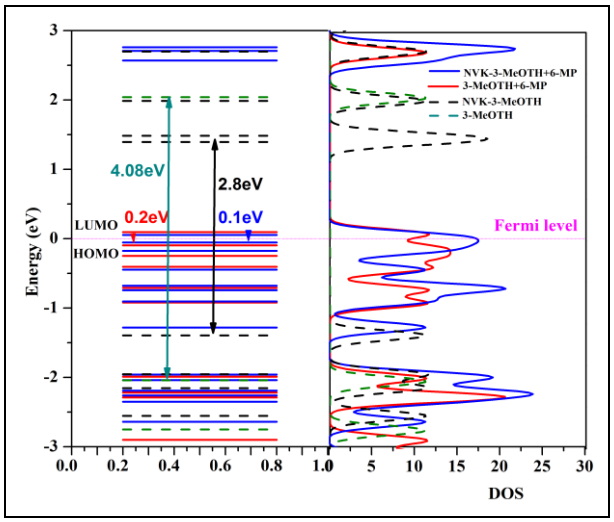

Fig. 3: Schematic view of HOMO-LUMO gap (left panel) and DOS profiles (Right panel) of 3-MeOTH and 3-MeOTH-NVK matrices before and after adsorption of 6-MP drug

The study analyzed conductance and detection range through transmission spectra of 6-MP adsorbed 3-MeOTH and 6-MP adsorbed 3-MeOTH-NVK systems to validate the suitability of the reduced E_H-E_L gap for drug sensing. A two-probe simulation system featuring gold electrodes was used in the device (Fig.4) (Xue *et al.* 2008). A detailed analysis of conductance through the transmission spectrum of the studied systems is shown in Fig. 5. The adsorption of 6-MP results in nearly a threefold enhancement in amplitude for the peaks of 3-MeOTH (Fig. 5a). Moreover, a peak in the range 0.2eV to -0.3eV indicates a change in conductivity. The greater amplitude suggests an increase in conductance(Agrawal *et al.* 2021). Fig. 5b compares 6-MP adsorbed 3-

MeOTH-NVK with 6-MP adsorbed 3-MeOTH and shows peak amplitude enhancement between 0.1eV to -0.2eV. Moreover, two additional peaks appear at -0.6 eV and -0.7 eV with notable amplitudes, affirming the enhanced conductance of the 3-MeOTH-NVK copolymer for the 6-MP drug. This enhanced conductance is substantiated by a reduced E_H-E_L gap.

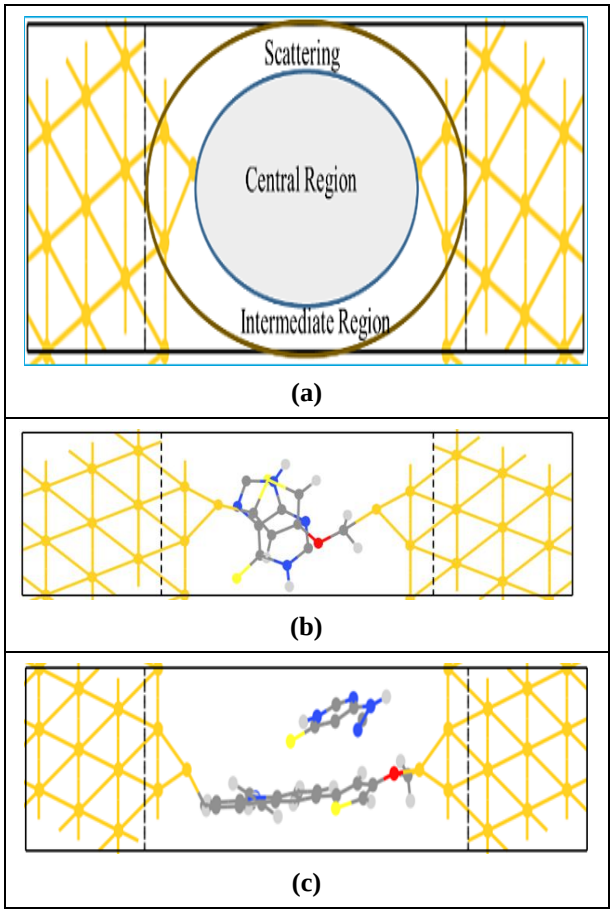

Fig. 4: (a) Two-probe semi-infinite linear and 3×3×2 gold (Au) chain electrodes with (b) 3-MeOTH+6-MP and (c) 3-MeOTH-NVK+6-MP

Further analysis is directed towards examining variations in conductance within the studied systems concerning the spatial distance between the 6-MP drug and the 3-MeOTH and 3-MeOTH-NVK matrices, particularly within the optimized adsorption range. An inverse relationship between conductance and the distance of the 6-MP drug to the matrices within the optimized adsorption range is observed (Fig. 6), highlighting the sensitivity of both matrices in the presence of the 6-MP drug. Utilizing Equation 3 (Agrawal *et al.* 2021) (Table 2), the sensitivity of these matrices to the 6-MP drug was calculated. The resulting sensitivities for 3-MeOTH+6-MP and 3-MeOTH-NVK+6-MP are 34.24% and 72.04%, respectively, confirming the significant sensitivities exhibited by both matrices. Notably, 3-MeOTH-NVK+6-MP demonstrates a 37.8% higher sensitivity compared to 3-MeOTH+6-MP system.

$$S = G\text{-}G_0/G \quad \text{..... (3)}$$

Here, G represents the conductance of the 6-MP adsorbed system, and G_0 is the conductance of the matrix.

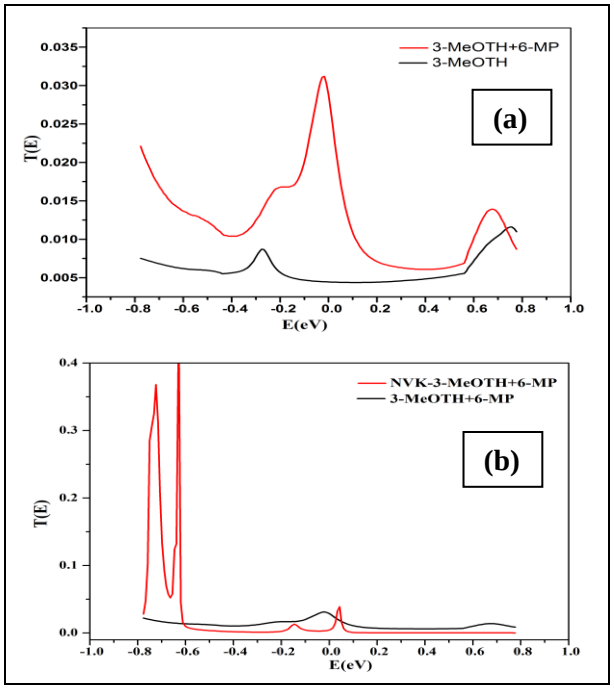

Fig. 5: Comparative transmission spectrum of (a) 3-MeOTH and 3-MeOTH+6-MP, and (b) 3-MeOTH+6-MP and 3-MeOTH-NVK+6-MP

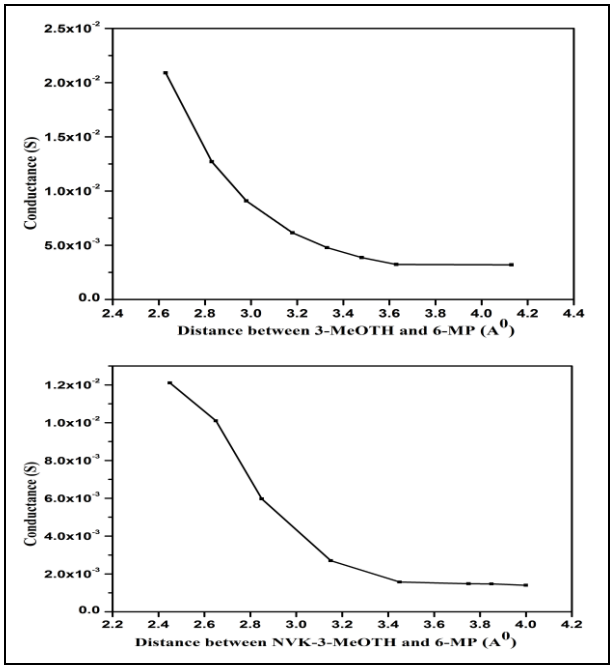

Fig. 6: Conductance vs distance graph of (a) 3-MeOTH+6-MP and (b) 3-MeOTH-NVK +6-MP systems

Table 2. Conductance and sensitivity of 3-MeOTH, 3-MeOTH-NVK, 3-MeOTH+6-MP, and 3-MeOTH-NVK+6-MP systems

System	Conductance (mS)	Sensitivity (%)
3-MeOTH	3.14	-
3-MeOTH+6-MP	4.78	34.24
3-MeOTH-NVK	1.67	-
3-MeOTH-NVK+6-MP	5.97	72.04

4. CONCLUSION

Computational analyses reveal that 3-MeOTH-NVK is a more reliable matrix for detecting the 6-MP drug than 3-MeOTH. This superiority arises from the 6-MP adsorption on 3-MeOTH-NVK being 1.6 times more stable and involving two-fold charge transfer than with 3-MeOTH. This transformation is supported by the MES and DOS profile, along with approximately 55% conductivity enhancement in the 3-MeOTH-NVK+6-MP system compared to the 3-MeOTH+6-MP system, as calculated using transmission spectra. The sensitivity to the 6-MP drug is significantly enhanced to 37.8% through the copolymerization of 3-MeOTH with NVK. The combination of improved conductance and significant sensitivity establishes 3-MeOTH-NVK as a reliable sensor for detecting the 6-MP drug.

FUNDING

This research received no specific grant from any funding agency in the public, commercial, or not-for-profit sectors.

DECLARATION OF COMPETING INTEREST

The author declares no conflict of interest in the presentation of this research.

ACKNOWLEDGEMENT

Our sincere gratitude is extended to the Material Synthesis and Sensor Design (MSSD) Lab at Atal Bihari Vajpayee-Indian Institute of Information Technology and Management (ABV-IIITM), Gwalior, for their invaluable support with computational infrastructure.

COPYRIGHT

REFERENCE

Agrawal, S., Kaushal, G., and Srivastava, A. , Electron transport in C3N monolayer: DFT analysis of volatile organic compound sensing, *Chem. Phys. Lett*., 762, 138121 (2021). https://doi.org/10.1016/j.cplett.2020.138121

Agrawal, S., Srivastava, A., Kaushal, G., and Srivastava, A., Edge Engineered Graphene Nanoribbons as Nanoscale Interconnect: DFT Analysis, *IEEE Trans. Nanotechnol*., 21, 43–51 (2022). https://doi.org/10.1109/TNANO.2021.3140041

Ensafi, A. A., and Karimi-Maleh, H. , Determination of 6-mercaptopurine in the presence of uric acid using modified multiwall carbon nanotubes-TiO2 as a voltammetric sensor, *Drug Test. Anal*., 4(12), 970–977 (2012). https://doi.org/10.1002/dta.286

González-Burciaga, L. A., García-Prieto, J. C., García-Roig, M., Lares-Asef, I., Núñez-Núñez, C. M., and Proal-Nájera, J. B. , Cytostatic drug 6-mercaptopurine degradation on pilot scale reactors by advanced oxidation processes: Uv-c/h2o2 and uv-c/tio2/h2o2 kinetics, *Catal*., 11(5) (2021). https://doi.org/10.3390/catal11050567

Hatamluyi, B., and Es'haghi, Z. ,Electrochemical biosensing platform based on molecularly imprinted polymer reinforced by ZnO–graphene capped quantum dots for 6-mercaptopurine detection, *Electrochimica Acta*, 283, 1170–1177 (2018). https://doi.org/10.1016/J.ELECTACTA.2018.07.068

Ipte, P. R., Manna, S., and Satpati, A. K. , Electrochemical and spectroscopic evaluation of 6-MP and its interaction with carbon dots and dsDNA, *Microchem. J.*, 184, 108159 (2023). https://doi.org/10.1016/J.MICROC.2022.108159

Mousavi, A., Zare-Dorabei, R., and Mosavi, S. H., A novel hybrid fluorescence probe sensor based on metal-organic framework@carbon quantum dots for the highly selective detection of 6-mercaptopurine, *Anal. Methods*, 12(44), 5397–5406 (2020). https://doi.org/10.1039/d0ay01592j

Saboorizadeh, B., Zare-Dorabei, R., and Shahbazi, N. , Green synthesis of carbon quantum dots and their application as a fluorometric sensor for highly selective determination of 6-mercaptopurine in biological samples, *J. Taiwan Inst. Chem. Eng*., 129, 389–395 (2021). https://doi.org/10.1016/J.JTICE.2021.09.015

Santana-Viera, S., Montesdeoca-Esponda, S., Sosa-Ferrera, Z., and Santana-Rodríguez, J. J., Cytostatic drugs in environmental samples: An update on the extraction and determination procedures, *TrAC, Trends Anal. Chem*., 80, 373–386 (2016). https://doi.org/10.1016/J.TRAC.2015.08.016

Sharma, P., Khare, K. P., Srivastava, R., Srivastava, A., and Kathal, R., Structural and electronic properties of n-vinylcarbazole - 3-methoxythiophene copolymer: DFT analysis, *J. Phys. Conf. Ser*., 2663(1), 012030 (2023). https://doi.org/10.1088/1742-6596/2663/1/012030

Tajik, S., Beitollahi, H., Jang, H. W., and Shokouhimehr, M., A screen printed electrode modified with Fe3O4@polypyrrole-Pt core-shell nanoparticles for electrochemical detection of 6-mercaptopurine and 6-thioguanine, *Talanta*, 232, 122379 (2021). https://doi.org/10.1016/J.TALANTA.2021.122379

Xue, Y., and Mansoori, G. A., Quantum conductance and electronic properties of lower diamondoid molecules and derivatives, *Int. J. Nanosci*., 7(1), 63–72 (2008). https://doi.org/10.1142/S0219581X08005183